Noncircular converging flows in viscous gravity currents

J. A. Diez, L. P. Thomas, S. Betelú, R. Gratton, and B. Marino
Instituto de Física Arroyo Seco, Facultad de Ciencias Exactas, Universidad Nacional del Centro de la Provincia de Buenos Aires, Pinto 399, 7000 Tandil, Argentina

J. Gratton
Instituto Nacional de Física de Plasmas, Consejo Nacional de Investigaciones Cientificas y Tecnicas, Laboratorio de Fisica de Plasma, Departamento de Física, Facultad de Ciencias Exactas y Naturales, Universidad de Buenos Aires, Pabellón I, Ciudad Universitaria, 1428 Buenos Aires, Argentina

D. G. Aronson
School of Mathematics, University of Minnesota, Minneapolis, Minnesota 55455

S. B. Angenent
Department of Mathematics, University of Wisconsin, Madison, Wisconsin 53706
(Received 1 April 1998)

We study the filling of a dry region (cavity) within a viscous liquid layer on a horizontal plane. In our experiments the cavities are created by removable dams of various shapes surrounded by a silicon oil, and we measure the evolution of the cavity's boundaries after removal of the dams. Experimental runs with circular, equilateral triangular, and square dams result in circular collapse of the cavities. However, dams whose shapes lack these discrete rotational symmetries, for example, ellipses, rectangles, or isosceles triangles, do not lead to circular collapses. Instead, we find that near collapse the cavities have elongated oval shapes. The axes of these ovals shrink according to different power laws, so that while the cavity collapses to a point, the aspect ratio is increasing. The experimental setup is modeled within the lubrication approximation. As long as capillarity is negligible, the evolution of the fluid height is governed by a nonlinear diffusion equation. Numerical simulations of the experiments in this approximation show good agreement up to the time where the cavity is so small that surface tension can no longer be ignored. Nevertheless, the noncircular shape of the collapsing cavity cannot be due to surface tension which would tend to round the contours. These results are supplemented by numerical simulations of the evolution of contours which are initially circles distorted by small sinusoidal perturbations with wave numbers $k \geq 2$. These nonlinear stability calculations show that the circle is unstable in the presence of the mode $k=2$ and stable in its absence. The same conclusion is obtained from the linearized stability analysis of the front for the known self-similar solution for a circular cavity.
[S1063-651X(98)04711-4]

PACS number(s): 47.50.+d

I. INTRODUCTION

This work concerns convergent viscous gravity currents, which occur when a viscous layer on a horizontal surface fills an initially dry region (cavity). As time progresses, the fluid spreads into this region and at some time t_c (closure or focusing time), the fluid fills the cavity. An important feature of these currents is that the flow is primarily horizontal and is governed by a balance between gravity and viscous forces, inertia effects being negligible. This problem with radial symmetry (circular cavity) has received attention in recent years [1–7]. It is known that for time t less than but close to t_c and sufficiently small distances r from the center of symmetry, the fluid height $h(r,t)$ is described by a self-similar function [5,6]. Self-similar behavior also occurs for $t \gtrsim t_c$ in the neighborhood of $r=0$.

Recently [8], it has been shown that there can be local self-similar behavior which is not axially symmetric in the post-focusing stage. However, no description of the nonaxially symmetric closure process is known. Qualitatively, it seems reasonable to guess that near the closure the system should behave in a simple general way, largely independent of the initial and far-field conditions. In addition, the cavity contour should advance faster where the inward curvature is larger, since ∇h is larger there. Both guesses are experimentally confirmed here, but the results show that they do not imply that the contour always tends asymptotically to a circle or any self-similar form.

We approach the problem in several steps. First, we perform experiments with a silicon oil on a glass surface and create the cavity by means of dams of various shapes. Surprisingly, we find that some special shapes of the dams do not result in circular collapsing flows (see below), but in collapsing contours shaped as elongated ovals. We also compare the measurements with the results of a numerical code which gives the time evolution of the flow, assuming that surface tension effects (inevitably present in the experiments) are negligible. The comparison shows that surface tension affects the evolution of the contours mainly in the regions where their inwards curvature becomes of the order of the capillary length a. However, surface tension effects cannot be responsible for the appearance of noncircular collapsing flows since, on the contrary, the tendency of capillary forces is to round the contours.

The experiments and numerical simulations suggest that circular contours are not attracting. Consequently, we perform a series of numerical simulations to test the nonlinear stability of circular contours. In particular, we simulated the experimental setup, but now with dams of circular shape perturbed by sinusoidal modes having various azimuthal mode numbers k. The main result is that the collapsing contours become elongated only when the mode $k=2$ is present. Finally, we investigate the linear stability of the level sets of the known axially symmetric self-similar focusing solution, the so-called Graveleau solution [1]. These solutions describe to leading order the collapse of a circular cavity [5,6]. Our analysis shows that the circular interfaces of the Graveleau solutions are unstable to perturbations with wave numbers $k \leqslant 2$, and stable to perturbations with wave numbers $k \geqslant 3$. Thus, in particular at the level of linear analysis, elongation ($k=2$) induces instability. This is in agreement with the experimental observation, the numerical simulations, and the numerical nonlinear perturbation analysis cited above.

II. EXPERIMENTS AND NUMERICAL SIMULATIONS

In the experiments the flow is produced in a flat glass tray ($72\times 94\times 10$ cm^3). The horizontality of the bottom plate is optically controlled up to 0.01 cm. A layer (thickness $h_0 \cong 0.5$ cm) of polydimethylsiloxane (PDMS, $\nu=101.6$ cm^2/s, $\rho=0.973$ g/cm^3, $\gamma=21$ dyn/cm at $T=20\,^\circ$C) initially surrounds a central dry region (the cavity) bounded by a dam which is raised at $t=0$. A video camera records from below the evolution of the dry region contour and data are obtained by digitalizing a set of selected frames (the resolution attainable with the maximum zoom is about 0.01 cm).

We employ dams shaped as circles, squares, equilateral triangles, and the figures that result from the elongation of these regular contours along a symmetry axis, i.e., ellipses, rectangles and rhombs, and isosceles triangles. The area of the initial dry region (≈ 100 cm^2) is a small fraction of the total tray area. Experiments with elongated dams were repeated for different orientations of the major axis with respect to the tray walls. These changes never produced appreciable effects. The experimental results are well reproducible; the main sources of dispersion are the pixel size and, in the initial stage, the formation of bubbles and other perturbations associated with the removal of the dam.

The experiments with circular dams confirm with improved accuracy the results reported in Ref. [4]. Therefore, in this short overview we pass directly to experiments with elliptical dams. In Fig. 1, we show a temporal sequence of contours for a case with initial radii $r_{\max}(0)=10$ cm and $r_{\min}(0)=5$ cm. A noteworthy point is that the contours are close but not equal to ellipses. In Fig. 2, we plot $r_{\max}(t)$ and $r_{\min}(t)$ (the lines correspond to numerical simulations; see below). It is seen that the cavity becomes more and more elongated [i.e., the aspect ratio $A(t)=r_{\max}/r_{\min}$ increases as the size decreases] until finally it resembles a rapidly shortening narrow oval (the width falls below the resolution while the length is still of the order of a millimeter). Note that this occurs despite the fact that the contour velocity is larger in the regions of larger curvatures as expected (near the apexes). This is also shown by the curve corresponding to this case in Fig. 3, where we report $\Delta r(t)=r_{\max}-r_{\min}$ both from experiments and simulations.

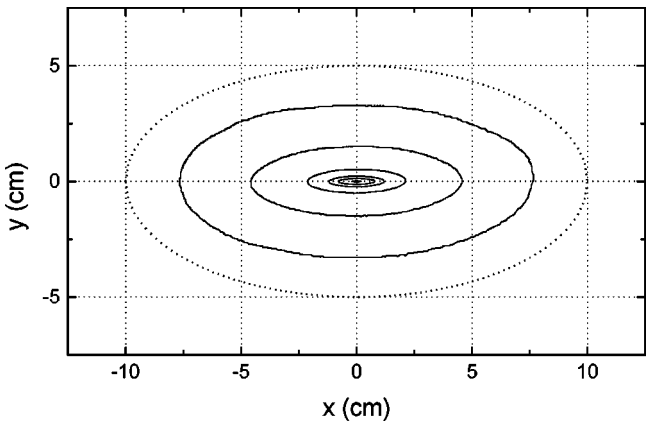

FIG. 1. Temporal sequence of experimental contour shapes for an elliptical dam [$r_{\max}(0)=10$ cm, $r_{\min}(0)=5$ cm] at $t=29.5$, 104.3, 157.0, 171.6, 176.5, and 182 s. The height of the fluid layer is $h_0=0.52$ cm and the closure occurs at $t_c=182.3$ s.

Before discussing the results with the other dam shapes, it is convenient to consider the mathematical modeling of the flow. It is well known [2,9,10] that when the free surface slopes are small, the lubrication approximation holds and consequently a nonlinear diffusion equation of the form [11]

$$\frac{\partial h}{\partial t}=\frac{\rho g}{3\mu}\,\nabla\cdot(h^3\nabla h) \tag{1}$$

describes the height profile $h(x,y,t)$, where μ is the viscosity, ρ the density, and g the gravity. The effects of surface tension have not been included, because they do not appre-

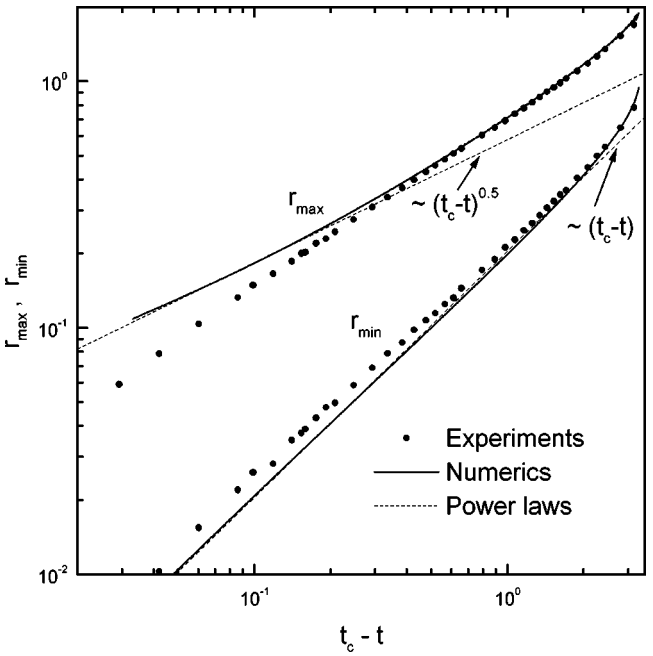

FIG. 2. Major ($r_{\max}$) and minor ($r_{\min}$) radius of the collapsing cavity of Fig. 1 as a function of t_c-t. The radii and the time are in units of $r_{\min}(0)$ and $t_0=3\mu r_{\min}(0)^2/\rho g h_0^3$ ($=54.4$ s), respectively. The symbols represent the experimental data and the lines correspond to the numerical simulations [13] with different values of $\Delta x_{\min}=\Delta y_{\min}$ also in units of $r_{\min}(0)$.

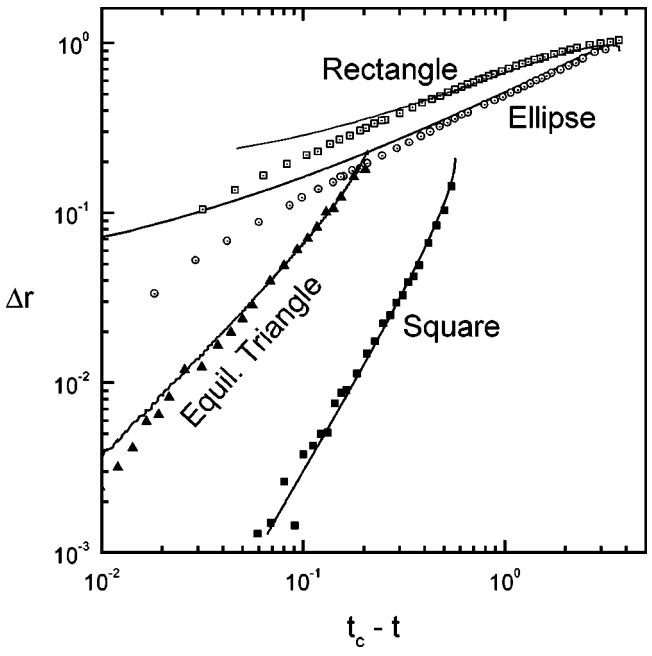

FIG. 3. Absolute departure from circularity $\Delta r = r_{max} - r_{min}$ as a function of $t_c - t$ in units of $r_{min}(0)$ and t_0, respectively, as in Fig. 2. The symbols represent the experimental data and the lines correspond to the numerical simulation [13].

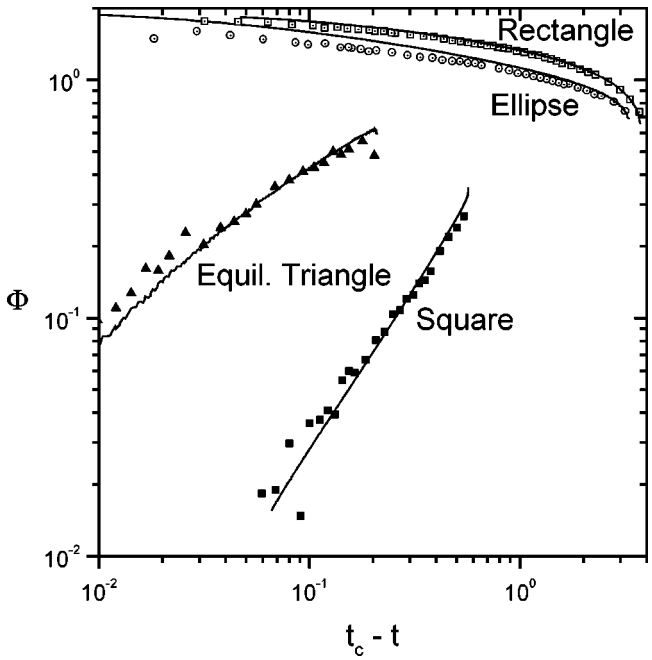

FIG. 4. Relative amplitude Φ as a function of $t_c - t$ in units of t_0 (see caption of Fig. 2). The symbols represent the experimental data and the lines correspond to the numerical simulation [13].

ciably affect the global flow dynamics provided the size of the region is much larger than the capillary length $a = \sqrt{\gamma/\rho g} \cong 0.15$ cm (see, for instance, Ref. [12]).

In addition, we have developed a numerical code to solve Eq. (1) in Cartesian coordinates inside a rectangular domain [13]. It is implemented in finite differences and employs the alternating-direction implicit method (see, for example, Ref. [14]). The code uses a nonuniform grid and was validated by comparison with both the circular diverging [15,16] (drop spreading) and circular converging [1,4,7] (filling of a cavity) solutions. Some special diverging noncircular solutions [17] were also accurately calculated. To achieve a high resolution of the contour near the closure, the simulations were carried out in a grid of 200×200 points with the smallest cells located at the center [$\Delta x_{min} = \Delta y_{min} = 0.002$ in units of $r_{min}(0)$]. The calculations were performed on a workstation (Silicon Graphics Indy) and each run took about two hours. For a particular case (initial elliptic contour of aspect ratio 2), we performed a more accurate simulation (551×551 grid points) which took about 15 days.

Figure 2 shows a good agreement between the experimental and numerical values of r_{min}, and its asymptotic evolution is closely approximated by a power law with an exponent very close to unity. The behavior of r_{max} suggests a power-law dependence with an exponent considerably lower than unity (≈ 0.5). An accurate determination of that exponent would require a much more extensive numerical simulation, mainly because the curvature radius at the apexes becomes very small near the closure, thus reducing the precision of the numerical simulation there. The results with three different grids are shown in Fig. 2. Note that there is a strong and progressive departure between experimental and numerical values of r_{max}. This is interpretable as an effect of surface tension, which becomes important when the radius of curvature R at the apexes is of the order of the capillary length a. In fact, by assuming an elliptical contour, we may estimate $R \cong r_{min}^2 / r_{max}$. R is close to 0.15 cm for $r_{max} \approx 3$ cm and $r_{min} \approx 0.75$ cm, the range where the departure becomes appreciable. Physically, we expect that surface tension tends to smooth the curvature distribution, thus keeping the aspect ratio below the numerical values and preventing its unbounded increase near the collapse.

The experiments with squares and equilateral triangles lead to circular closures which in the last stage do not differ from those originating from circular dams. The disparity between the experimental and numerical values of $r_{max}(t)$ and $r_{min}(t)$ are much less than in the above elliptical case. This is reasonable since the curvature tends to a uniform distribution regardless of capillary effects. Instead, rhombic and rectangular dams, as well as dams shaped as isosceles triangles, lead to noncircular closures, reminiscent of those originating from elliptical dams. Therefore, we center our interest on the time evolution of $\Delta r(t) = r_{max} - r_{min}$. In Fig. 3, we report $\Delta r(t)$ for a square dam (side 10 cm), an equilateral triangle dam (side 12 cm), a rectangular dam (20×10 cm^2), and the elliptical dam of Fig. 2. In the rectangular and elliptical cases, the decrease of $\Delta r(t)$ is far slower than in the cases of regular shapes. This difference has the significant consequence shown in Fig. 4. The relative departure from circularity, defined as

$$\Phi = \frac{\Delta r}{r_{av}} = \frac{r_{max} - r_{min}}{(r_{max} + r_{min})/2}, \tag{2}$$

decreases for the dams of regular shapes and increases for the dams with elongated shapes.

In summary, the results strongly indicate that an elon-

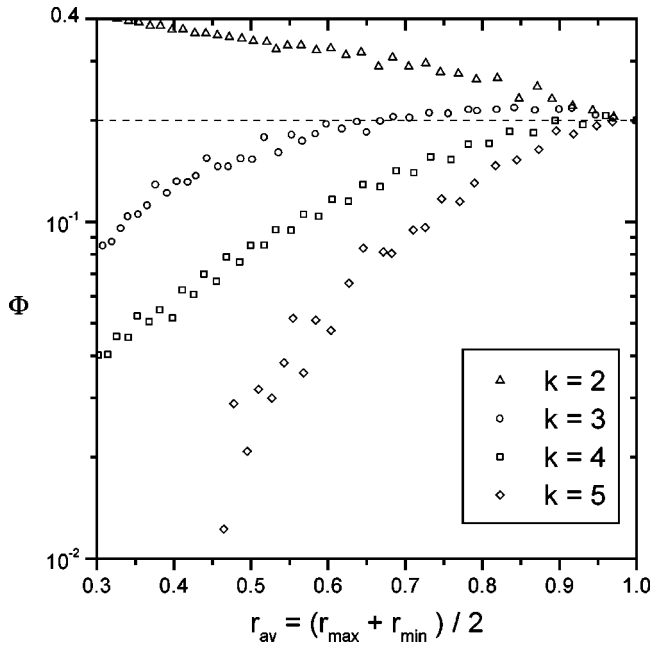

FIG. 5. Relative amplitude Φ as a function of r_{av} in units of $r_{\mathrm{min}}(0)$ for small perturbations of a circle with different modes $k=2$, 3, 4, and 5.

gated contour does not evolve to a circular shape. Specifically, both r_{min} and r_{max} tend to zero simultaneously at $t=t_c$ following different power laws on $t-t_c$. Consequently, the departure from circularity Φ increases as the cavity closes. The results cannot be attributed either to experimental or to numerical effects not contained in the lubrication approximation on the basis of Eq. (1). Regarding the experimental results, the effects of surface tension are the critical issue, since the front positions are determined with high accuracy (<0.1 mm) and the effects related to lacks of planarity or horizontality of the tray have been shown to be negligible. However, surface tension cannot be responsible for the increase of Φ, since, on the contrary, it tends to reduce Φ. In fact, Fig. 4 shows that the experimental data are a little below the numerics for the ellipse and the rectangle. The reliability of the numerics is shown in Fig. 2 since the results for three different grid sizes are practically coincident. As a consequence, the behavior of the noncircular collapses is well determined by the experiments and the numerics. Perhaps the most significant uncertainty regards the value of the exponent for the time dependence of r_{max}, which certainly is much less than unity and appears to be close to 0.5.

III. STABILITY OF PERTURBED CIRCULAR CONTOURS

In order to provide an interpretative scheme to these results, we perform numerical simulations starting with a distorted circular contour given by

$$r=1+\delta\cos(k\theta), \quad \delta=0.1, \quad k=2,3,4,5 \tag{3}$$

with r and θ the polar coordinates. As shown in Fig. 5, Φ increases for $r_{\mathrm{av}}\to 0$ only for $k=2$, so that only in this case does the contour tend to elongated ovals, otherwise it tends to circles. For much smaller δ ($\lesssim 0.01$) and $k=2$, the aspect ratio $A(t)$ remains almost constant and equal to $A(0)\cong 1$ during most of the collapse, as should be expected because the amplitude of the distortion actually decreases. Only very near the closure ($r_{\mathrm{av}}\approx\delta$) does $A(t)$ increase rapidly and unboundedly. In the experiments with initial regular contours, some small $k=2$ distortions cannot be ruled out as a consequence of the removal of the dam; nevertheless, we obtain circular closures. This is because small distortions are overcome by capillarity before their effects on the aspect ratio become significant. Only those with amplitude δ much larger than the capillary length a may lead to noncircular closures. It is worth noting that the observed growth of the aspect ratio is not related to a true instability of the contour because the absolute amplitude Δr of all the deformation modes, including the $k=2$ mode, decreases in time.

These conclusions are further strengthened by the linear stability analysis of the level sets of the known axially symmetric self-similar focusing solutions to Eq. (1) (Graveleau solutions). These solutions describe, to leading order, the collapse of a circular interface [5,6]. In order to study focusing solutions to Eq. (1), it is convenient to introduce a new dependent variable

$$v=\frac{h^3}{3}$$

so that Eq. (1) becomes

$$\frac{\partial v}{\partial t}=3v\nabla^2 v+|\nabla v|^2. \tag{4}$$

If we normalize the focusing time to be $t_c=0$ ($t<0$), then the Graveleau solutions form a one-parameter family of self-similar solutions given by

$$g_b(\mathbf{x},\mathbf{t})=-\frac{|\mathbf{x}|^2}{\mathbf{t}}\,\varphi(\mathbf{b}\eta),$$

where $\eta=t/|\mathbf{x}|^{\alpha}$ is the similarity variable and the similarity exponent α lies between 1 and 2 (see Ref. [7]; $\alpha=1.312\ldots$ for the Graveleau solution). The focusing occurs since $\varphi(0)=0$ and there is a $\gamma<0$, such that

$$\varphi(\eta)\begin{cases}>0 & \text{for } \gamma<\eta<0\\ =0 & \text{for } \eta\leqslant\gamma.\end{cases}$$

Moreover, $\varphi'(0)=-1$, so that

$$\lim_{t\to 0} g_b(\mathbf{x},\mathbf{t})=\mathbf{b}|\mathbf{x}|^{2-\alpha}.$$

In the self-similar variables,

$$\mathbf{y}=\mathbf{x}(-\mathbf{t})^{-1/\alpha}, \quad \tau=-\ln(-t),$$

Eq. (4) becomes

$$\frac{\partial V}{\partial \tau}=3V\Delta V-\frac{\mathbf{v}}{\alpha}\cdot\boldsymbol{\nabla}V+|\nabla V|^2+\left(\frac{2}{\alpha}-1\right)V, \qquad (5)$$

where $V(\mathbf{y},\tau)=(-\mathbf{t})^{1-2/\alpha}\mathbf{v}(\mathbf{x},\mathbf{t})$. The Graveleau solutions are given by

$$g_b(\mathbf{x},\mathbf{t})=(-\mathbf{t})^{2/\alpha-1}\psi_{\mathbf{b}}(\rho),$$

with $\rho=|\mathbf{y}|$ and $\psi_b(\rho)=\rho^2\varphi(-b\rho^{-\alpha})$. Note that $\psi_b(\rho)$ is an axisymmetric steady-state solution to Eq. (5).

Let $V(\mathbf{y},\tau)$ be a solution to Eq. (5). We introduce polar coordinates (ρ,θ) in the $\mathbf{y}$ plane, and write $V(\mathbf{y},\tau)=\mathbf{W}(\rho,\theta,\tau)$. Since we are interested in the stability of circular fronts, it is useful to work with the equation for the evolution of the level curves derived from Eq. (5). Specifically, we invert $p=W(\rho,\theta,\tau)$ to obtain $\rho=S(p,\theta,\tau)$ and derive the equation for S. We refrain from writing down this very complicated nonlinear partial differential equation, since we are only interested in its linearization about the level curves for the Graveleau solution. Let $\Psi(p)$ denote the inverse of the Graveleau solution $\psi_1(\rho)$ so that

$$\psi_1(\Psi(p))=p,$$

and retain only the linear terms in the equation for

$$\zeta(p,\theta,\tau)=S(p,\theta,\tau)-\Psi(p).$$

Finally, if we set

$$\zeta(p,\theta,\tau)=A(p)\exp(\delta\tau+ik\theta),$$

we obtain the equation

$$3p\Psi^2A''+\left[\left(\frac{2}{\alpha}\Psi\Psi'-1\right)\Psi^2-6p\Psi\Psi'-3p\left(\frac{2}{\alpha}-1\right)(\Psi\Psi')^2\right]A'+\left[3p(1-k^2)+\left(\frac{1}{\alpha}-\delta\right)\Psi^2\right]\Psi'^2A=0. \qquad (6)$$

Equation (6) has a regular singular point at $p=0$ and possesses a unique smooth solution satisfying

$$A(0)=1. \qquad (7)$$

For $p\gg 1$, Eq. (6) has a solution with algebraic growth and a solution with superexponential growth. For each wave number k the eigenvalue δ is selected so that the solution of Eq. (6) satisfying Eq. (7) has algebraic growth at infinity. In general, we cannot find δ analytically and so we must resort to a numerical shooting technique to determine it (for details, see Ref. [18]).

It is clear that the Graveleau level curves are unstable to perturbations with wave numbers $k=0$ and 1 which correspond to perturbing the location of the focusing point and the radius of the initial circle. Our numerical and theoretical studies show that the Graveleau level curves are unstable with respect to perturbations with wave number $k=2$, and stable for $k>2$. These results are consistent with the experiments and simulations described above.

IV. FINAL REMARKS

The present results show that nonaxially symmetric converging flows differ from the well known symmetric case in many nontrivial ways. The full understanding of this complicated problem requires theoretical developments clearly beyond the scope of the present work. However, it is already apparent that no simple generalizations based on the circular case can be made. Very near the collapse, the shape of the contour for elongated dams always resembles a narrow oval, thus suggesting an asymptotic behavior largely independent of the initial conditions. However, this behavior is not self-similar since different power laws hold for $r_{\min}$ and $r_{\max}$. Indeed, both of these radii tend to zero as $t\to t_c$ although the aspect ratio $A\to\infty$.

A natural extension of the present work is to study the behavior of Eq. (1) with a nonlinearity exponent different from $m=3$, since these other equations appear in many situations of considerable practical interest [9,19,20], for instance flow in porous media ($m>1$). However, these situations are not amenable to simple experimental study, and have not been considered here.

ACKNOWLEDGMENTS

This work was supported in part by the Consejo Nacional de Investigaciones Científicas y Técnicas (CONICET) and the Comisión de Investigaciones Científicas de la Provincia de Buenos Aires (CICPBA). D.G.A. was supported in part by NSF Grant No. DMS 9503392. S.B.A. was supported in part by NSF PYI Grant No. DMS 9058492.

[1] J. Graveleau, Report Interne C.E.A., 1972 (unpublished).
[2] J. Gratton and F. Minotti, J. Fluid Mech. **210**, 155 (1990).
[3] J. Diez, J. Gratton, and F. Minotti, Q. J. Mech. Appl. Math. **50**, 401 (1992).
[4] J. Diez, R. Gratton, and J. Gratton, Phys. Fluids A **4**, 1148 (1992).
[5] S. B. Angenent and D. G. Aronson, Phys. Fluids **7**, 223 (1995).
[6] S. B. Angenent and D. G. Aronson, Commun. Partial Diff. Equations **20**, 1217 (1996).
[7] D. G. Aronson and J. Graveleau, Euro. J. Appl. Math. **4**, 65 (1993).
[8] S. B. Angenent and D. G. Aronson, Euro. J. Appl. Math. **7**, 277 (1996).
[9] H. E. Huppert, J. Fluid Mech. **173**, 557 (1986).

[10] G. I. Barenblatt, Izv., Acad. Sci., USSR, Atmos. Oceanic Phys. **14**, 139 (1978).
[11] J. Buckmaster, J. Fluid Mech. **81**, 735 (1977).
[12] B. Marino, L. Thomas, J. Diez, and R. Gratton, J. Colloid Interface Sci. **177**, 14 (1996).
[13] J. Diez and S. Betelú (unpublished).
[14] W. H. Press, S. A. Teukolsky, W. T. Vetterling, and B. P. Flannery, *Numerical Recipes in Fortran* (Cambridge Univ. Press, Cambridge, 1992).
[15] G. I. Barenblatt, Prikl. Mat. Mekh. **16**, 67 (1952).
[16] R. E. Pattle, Q. J. Mech. Appl. Math. **12**, 407 (1959).
[17] S. Betelú (unpublished).
[18] S. B. Angenent and D. G. Aronson (unpublished).
[19] R. C. Kerr and J. R. Lister, Earth Planet. Sci. Lett. **85**, 241 (1987).
[20] J. E. Simpson, Annu. Rev. Fluid Mech. **14**, 341 (1982).